metals

MDPI

Article

Competition for Nucleation and Grain Initiation during Solidification

Feng Gao and Zhongyun Fan *

Brunel Centre for Advanced Solidification Technology (BCAST), Brunel University London, Uxbridge UB8 3PH, Middlesex, UK
* Correspondence: zhongyun.fan@brunel.ac.uk

Abstract: Without the addition of any grain refiner, the inclusion particles in a melt will induce heterogeneous nucleation and grain initiation during the solidification of metallic materials. However, with grain refiner addition, the exogenous particles (from the grain refiner) and the native inclusions (e.g., oxide particles) will co-exist in the melt, and there will be competition for nucleation and grain initiation among different types of solid particles. In this paper, we analyze such competition in Al and Mg alloys using a numerical solidification model that we have developed previously. The numerical calculations show that the competition for nucleation is strongly dependent on nucleation undercooling of the different types of particles, while the competition for grain initiation is closely related to the sizes of solid particles. Based on the numerical results, the general rules of competition for nucleation and grain initiation have been developed: nucleation starts with particles of minimum nucleation undercooling, followed by particles with progressively larger nucleation undercooling; and grain initiation starts with solid particles of the largest size, followed by solid particles with progressively smaller sizes.

Keywords: nucleation; grain initiation; grain refinement; solidification

Citation: Gao, F.; Fan, Z. Competition for Nucleation and Grain Initiation during Solidification. *Metals* **2022**, *12*, 1512. https://doi.org/10.3390/met12091512

Academic Editor: Chang Yong Jo

Received: 9 August 2022
Accepted: 8 September 2022
Published: 13 September 2022

1. Introduction

Inclusions in an alloy melt, such as oxides and borides, may induce heterogeneous nucleation [1] and the subsequent grain initiation during the solidification of metallic materials. Grain refinement [2–5] is defined as the deliberate suppression of columnar grain growth in ingots and castings and the formation of a fine and equiaxed grain structure throughout the material. Grain refinement offers a unique opportunity for improving the performance of metallic materials, such as reduced cast defects in the solidified microstructure, simultaneously improved ductility and mechanical strength and enhanced corrosion resistance [6] through the finely dispersed and uniformly distributed second phase particles.

The approaches to grain refinement during casting processes include chemical inoculation with the addition of grain refiners and the application of external fields, such as ultrasonic treatment (UST) [7,8], electromagnetic stirring [9–11] and intensive melt shearing [12–17]. Among these methods, inoculation prior to the casting processes has been widely used in industry to deliver grain refinement [2–5] through the addition of a large number of potent nucleant particles that act as the nucleation sites. For example, the Al-5Ti-1B grain finer and Mg-33Zr master alloy are considered to have the highest grain refining efficiency for Al and Mg alloys, respectively [2,18]. It has been confirmed that potent TiB_2 (TiB_2 with Al_3Ti 2DC (two-dimensional compound)) particles in Al-5Ti-1B grain refiner [19] and Zr particles in Mg-33Zr master alloy [18] dominate the nucleation and grain initiation processes during solidification.

Due to the high oxidation potential of Al and Mg, molten Al and Mg alloys oxidize rapidly in contact with air, resulting in inclusions being dominated by oxides. For example,

there are 0.1–10 ppm Al_2O_3 for pure Al and 10–200 ppm MgO for pure Mg [20,21]. Although there are also some other inclusions, such as AlN and Mg_3N_2, formed during the melting and casting processes for Al and Mg alloys [22–24], the Al_2O_3 (or $MgAl_2O_4$) and MgO particles are the dominant inclusions in Al and Mg alloys, and most of them exist in the form of oxide films [12,25–30]. Without the addition of a grain refiner, these oxide inclusions act as heterogeneous nucleation sites for the primary phase. For example, native MgO and $MgAl_2O_3$ particles have been confirmed as the nucleation sites in Mg-Al alloys [12,30,31] and Al-Mg alloys [13]. However, these oxide films lead to a low effective number of grain initiation events, resulting in a coarse grain structure in the as-cast condition, because only one grain initiation event occurs in a film or an agglomerate. The approaches that can effectively disperse the oxides and hence increase the effective oxide particle number density will reduce the grain size of cast alloys. For example, the effective grain refinement of Mg alloys can be achieved by intensive melt shearing [12,14–16], which increases the number density of native MgO particles from 10^{14} m^{-3} to 10^{17} m^{-3} [32].

Oxide particles, such as MgO in Mg alloys, require relatively large nucleation undercooling, because the low nucleation potency originates from the large lattice misfit between the oxide and the primary phase [12,30,31,33]. When the grain refiner is added to the melt, taking Mg-33Zr master alloy for Mg alloys as an example, the Zr particles nucleate Mg first (at a higher temperature) and dominate the subsequent grain initiation process due to the small nucleation undercooling and high particle number density [34]. This may not leave any chance for MgO particles to participate in the nucleation process.

The final grain size of a solidified alloy is determined by the competition for nucleation and grain initiation among the different types of particles, both endogenous and exogenous [34]. In this paper, we study the competition for nucleation and grain initiation among the different types of particles, e.g., Zr and native MgO particles in Mg alloys and TiB_2/Al_3Ti particles and native Al_2O_3 in Al alloys, using a numerical model. Based on the numerical results, we derive the basic rules that govern the competition for nucleation and grain initiation, which can be used to guide the development of new grain refiners for Al and Mg alloys.

2. Heterogeneous Nucleation and Grain Initiation

2.1. Recent Advances in Heterogeneous Nucleation

Nucleation during solidification in practical metallic systems is heterogeneous due to the inevitable existence of solid inclusions in metallic melts [1], which is commonly analyzed by classical nucleation theory (CNT) [35–38]. The heterogeneous CNT considers the balance between the interfacial energy change and the volume free energy change during the creation of a spherical cap on a substrate and uses the contact angle as a measure of the nucleation potency of the substrate [1,39]. However, it is realized that the heterogeneous CNT is invalid for potent nucleating substrates with a small contact angle [40], and the nucleation kinetics cannot be accurately described by the CNT for efficient catalysis at low undercooling [41,42].

The epitaxial nucleation model [43] represents an alternative description of heterogeneous nucleation at the atomic level. It suggests that heterogeneous nucleation proceeds layer-by-layer through structural templating at the liquid/substrate interface, and, hence, the lattice misfit (f) at the interface between the solid and the substrate has a strong influence on nucleation undercooling (ΔT_n), i.e., ΔT_n increases with the increasing lattice misfit. Recently, it has been revealed that, at temperatures above the nucleation temperature, the atoms in the melt adjacent to a crystalline substrate become layered, and such interfacial layers may exhibit substantial in-plane atomic ordering, which is referred to as prenucleation [44,45]. Prenucleation leads to the formation of a two-dimensional (2D) ordered structure at the liquid/substrate interface [44,45], which is affected by the lattice misfit [44], the atomic level surface roughness [46] and chemical interactions [47] between the substrate and the solid. The outcome of prenucleation is a precursor for the subsequent heterogeneous nucleation. In addition, using molecular dynamics (MD) simulation, a

three-layer nucleation mechanism was developed for heterogeneous nucleation [48–51], which explicitly predicts that nucleation undercooling increases linearly with the increase in the lattice misfit [50,51], and this is in good agreement with Turnbull's crystallographic model [52] and Fan's epitaxial nucleation model [43].

2.2. Grain Initiation during Solidification

After nucleation, the 2D nucleus can potentially template the further growth of the solid, leading to the formation of a spherical cap on the substrate with a curvature at the liquid/solid interface specified by the undercooling [50]. If a spherical cap can grow isothermally at this temperature, it will become a grain, and this process is referred to as grain initiation. However, whether the solid particle can freely grow is governed by the free growth criterion [53]:

$$\Delta T_{gi} d = 4\Gamma \quad (1)$$

$$\Gamma = \gamma / \Delta S_v \quad (2)$$

where ΔT_{gi} is the grain initiation undercooling, d is the diameter of the solid particle which numerically equals the diameter of the nucleant particle; γ is the interfacial energy of the solid/liquid interface; ΔS_v is the entropy of fusion per unit volume; and Γ is the Gibbs–Thompson coefficient. It should be pointed out that the three-layer heterogeneous nucleation mechanism generates a 2D nucleus, while the CNT produces a 3D nucleus from which the solid phase may grow [50]. In fact, in the new description of the early-stage solidification, the classical heterogeneous nucleation (cap formation) has been redefined as grain initiation [50,54]. Equation (1) suggests that, for a given system, the grain initiation undercooling, ΔT_{gi}, only depends on the size of the solid particle, since γ and ΔS_v are constant.

In reality, a melt contains a population of nucleant particles with a log-normal size distribution [55] and may exhibit different grain initiation behaviors [54,56,57]. When the nucleant particle has a high nucleation potency, nucleation occurs at a higher temperature, and grain initiation starts at a lower temperature initially with the solid particle with the largest size and then with progressively smaller ones with decreasing temperatures until recalescence [53]. This grain initiation behavior is referred to as progressive grain initiation (PGI) [54,56,57]. For the particle with large nucleation undercooling, grain initiation may become explosive, i.e., explosive grain initiation (EGI) [54,56,57], where a group of solid particles initiate grains almost simultaneously, and the latent heat released by both heterogeneous nucleation and the initial free growth can cause an immediate recalescence, which stifles any further grain initiation events. If the nucleation undercooling is moderate, the grain initiation is most likely in the hybrid grain initiation (HGI) mode [54,56,57], where a group of large solid particles initiate grains simultaneously in an explosive manner, and this is followed by progressive grain initiation on smaller solid particles until recalescence. More details on the grain initiation behavior have been reported elsewhere [54,56,57].

3. Competition for Nucleation

In this section, we use numerical calculations to illustrate the competition for nucleation. The numerical model was modified on the basis of that in Ref. [54], allowing two types of nucleant particles to be inputted. The parameters used in the numerical model are shown in Table 1 [54,55,58,59].

For Al alloys without the addition of a grain refiner, the native Al_2O_3 particles are the dominant inclusions in the melt, which will nucleate α-Al and dominate the grain initiation process during solidification. It is assumed that there is only one type of particles, i.e., Al_2O_3, in the Al alloy melt without any grain refiner addition and that the oxide particles have a log-normal size distribution with a geometric mean of d_0 = 0.08 μm and a standard deviation of σ = 0.82 [60]. The calculated lattice misfit at the Al/ Al_2O_3 interface is 3.5% [61], which is larger than the misfit (0.09%) between potent TiB_2 (with Al_3Ti 2DC) and α-Al [19] but smaller than the misfit (7.9%) between MgO and α-Mg [30]. For the

numerical calculations, the nucleation undercooling (ΔT_n) of Al_2O_3 is assumed to be 0.3 K in this work.

Table 1. The parameters used in the numerical calculations. Data from Refs. [54,55,58,59].

Parameters (Symbol, Unit)	Al-Cu	Mg-Zr
Partition coefficient (k)	−2.5 [58]	4.7 [59]
Liquidus slope (m, K(wt.%)$^{-1}$)	0.13 [58]	8.2 [59]
Heat capacity (c_{pv}, Jm^{-3}K^{-1})	2.58×10^6 [55]	2.59×10^6 [54]
Enthalpy of fusion (ΔH_V, Jm^{-3})	9.5×10^8 [55]	6.75×10^8 [54]
Diffusion coefficient (D, m^{2}s^{-1})	2.52×10^{-9} [55]	2.7×10^{-9} [54]
Gibbs–Thompson coefficient (Γ, Km)	1.42×10^{-7} [55]	1.48×10^{-7} [54]
Volume (V_0, m^3)	1×10^{-6}	1×10^{-6}
Cooling rate (K/s)	3.5	3.5

Figure 1a shows the calculated cooling curve of Al-1Cu alloy without (blue solid line) and with (red dashed line) 1 ppt (0.1 wt.%) Al-5Ti-1B grain refiner at a cooling rate ($\dot{T}$) of 3.5 K/s. Without the addition of the grain refiner, only native Al_2O_3 particles exist in the melt, with the particle number density (N_0) of the oxides being estimated to be 10^{12} m^{-3}, which is two orders of magnitude less than MgO (10^{14} m^{-3}) in Mg alloys [20,21,32]. The maximum undercooling (ΔT_{max}) achieved without the grain refiner during solidification is 1.08 K (Figure 1a), and the calculated grain size is 357 μm. The grain initiation undercooling for the largest Al_2O_3 particle ("ΔT_{gi}(1st)") is 0.25 K (calculated from Equation (1) based on the N_0 (10^{12} m^{-3})), which is slightly smaller than the ΔT_n (0.3 K), indicating that the grain initiation is an HGI [54,56,57], i.e., EGI first, followed by PGI, as shown in Figure 1b. When 0.1 wt.% Al-5Ti-1B grain refiner is added in the Al-1Cu alloy, the N_0 of the potent TiB_2 particles (TiB_2 with Al_3Ti 2DC [19]) is 7.3×10^{12} m^{-3} [55], which have a log-normal size distribution with d_0 = 0.68 μm and σ = 0.876 [55]. The ΔT_n of the potent TiB_2 particle is estimated to be 0.01 K [53], which is smaller than the ΔT_{gi}(1st) (0.02 K calculated from Equation (1), based on the N_0 (7.3×10^{12} m^{-3})); grain initiation thus becomes fully PGI (Figure 1c). The ΔT_{max} (Figure 1a) achieved in Al-1Cu alloy is reduced to 0.21 K, and the calculated grain size is 105 μm. As the ΔT_n for Al_2O_3 is 0.3 K, which is larger than ΔT_{max} (0.21 K), the nucleation of α-Al on Al_2O_3 particles does not occur. Therefore, only the potent TiB_2 particles participate in the nucleation process.

A similar phenomenon happened in Mg alloys without and with the addition of Mg-Zr grain refiner. Figure 2a shows the calculated cooling curves of Mg-0.45Zr alloy without (blue solid line) and with (red dashed line) Mg-33Zr grain refiner at $\dot{T}$ = 3.5 K/s. Without the grain refiner addition, there are only native MgO particles in the melt, the N_0 of the MgO particles is estimated to be 10^{14} m^{-3} [32] and the size distribution is log-normal, with d_0 = 0.07 μm and σ = 0.45 [32]. The ΔT_{max} without the grain refiner addition is 1.82 K (Figure 2a), and the calculated grain size is 251 μm. The grain initiation undercooling for the largest MgO particle ("ΔT_{gi} (1st)") is 0.76 K, which is smaller than the ΔT_n (1.2 K [54]), indicating that the grain initiation is an HGI (Figure 2b). With the addition of Mg-33Zr grain refiner, the added Zr particles in the melt have an N_0 of 10^{12} m^{-3} and a log-normal size distribution with d_0 = 0.73 μm and σ = 0.62 [62]. The Zr particles will nucleate α-Mg first because of their high nucleation potency, followed by grain initiation (Figure 2c). The ΔT_{max} with grain refiner is 0.77 K (Figure 2a), which is smaller than the ΔT_n of MgO (1.2 K), meaning that the native MgO particles have no chance to participate in nucleation.

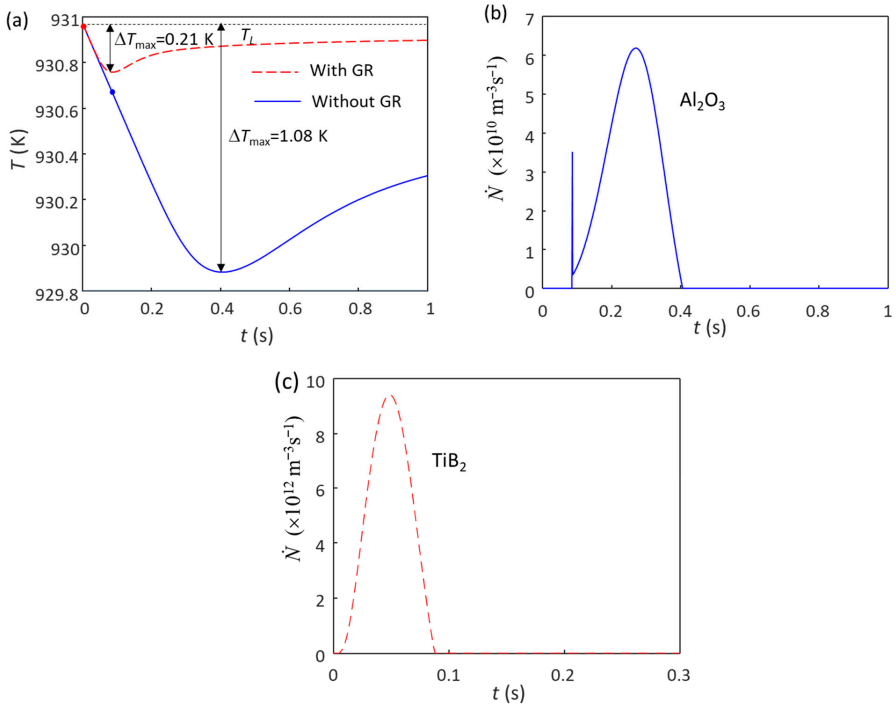

Figure 1. Solidification behavior of Al-1Cu alloy without and with the 1 ppt (0.1 wt.%) addition of Al-5Ti-1B grain refiner (GR) under a cooling rate of 3.5 K/s. (**a**) Cooling curves; (**b**) grain initiation rate without the addition of Al-5Ti-1B grain refiner; (**c**) grain initiation rate with the addition of Al-5Ti-1B grain refiner. The red and blue dots in (**a**) mark the onset of grain initiation on solid particles induced by TiB_2 and Al_2O_3 particles, respectively.

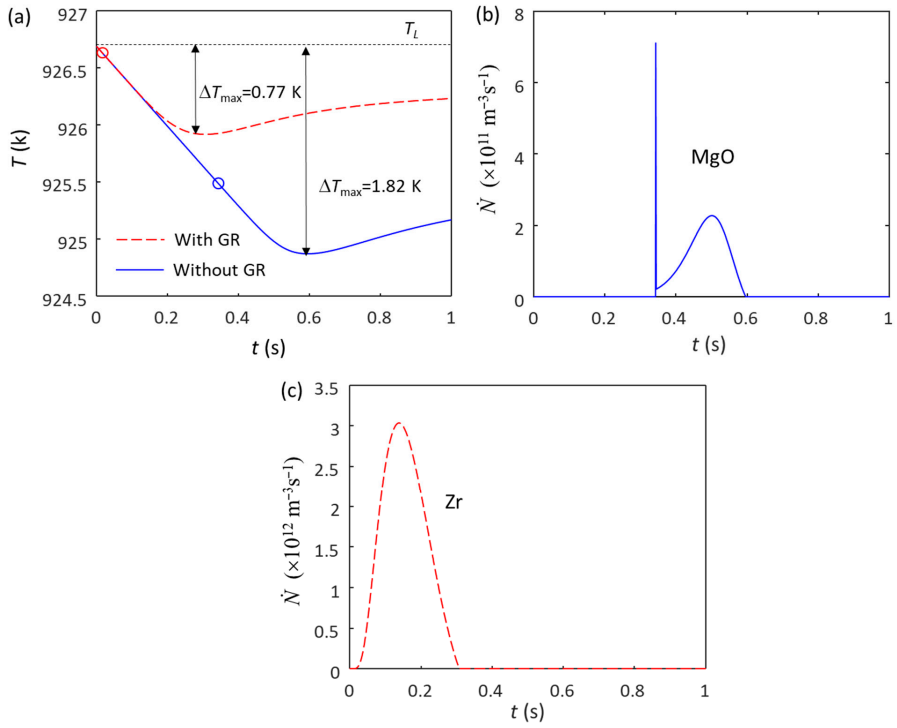

Figure 2. Solidification behavior of Mg-0.45Zr alloy without and with the addition of Mg-Zr grain refiner (N_0(Zr) = 10^{12} m^{-3}) under a cooling rate of 3.5 K/s. (**a**) Cooling curves; (**b**) grain initiation rate without the addition of Mg-Zr grain refiner; (**c**) grain initiation rate with the addition of Mg-Zr grain refiner. The red and blue dots in (**a**) mark the onset of grain initiation on solid particles induced by Zr and MgO particles, respectively.

The above two cases show the competition for nucleation between native oxide particles (Al_2O_3 and MgO) and potent particles (TiB_2/Al_3Ti and Zr) from grain refiners. Without the addition of grain refiners, the native oxide particles—Al_2O_3 in Al-1Cu alloy and MgO in Mg-0.45Zr alloy—are the only types of particles of significance, and they participate in both nucleation and the subsequent grain initiation processes (Figures 1b and 2b). When more potent particles are added to the melts, i.e., potent TiB_2 in Al-1Cu alloy and Zr in Mg-0.45Zr alloy, there is a competition for nucleation between the native oxide particles and the exogenous particles. Which type of particles can nucleate depends on the relative position of the nucleation undercooling of the individual type of particles. During solidification, the most potent nucleant particles will nucleate first, since they have the lowest nucleation undercooling. This will be followed by nucleation on particles that have progressively larger nucleation undercooling. All particles that satisfy $\Delta T_n < \Delta T_{max}$ will participate in nucleation, while those particles with $\Delta T_n > \Delta T_{max}$ will not be made for nucleation. In the previous two cases, we have $\Delta T_{max} < \Delta T_n$ (oxide); both Al_2O_3 and MgO particles fail in the competition for nucleation, and only the potent TiB_2 and Zr particles participate in the nucleation and grain initiation process (Figures 1c and 2c).

4. Competition for Grain Initiation

4.1. Competition for Grain Initiation between Potent TiB_2 and Al_2O_3 Particles in Al Alloys

Taking Al-4Cu alloy without a grain refiner as an example, Al_2O_3 particles are the dominant particles in the melt, which dominate the nucleation and grain initiation processes during solidification. Most of the Al_2O_3 particles are in the form of oxide films, and the effective N_0 of the Al_2O_3 particles is estimated to be 10^{12} m^{-3}. The application of intensive melt shearing can effectively disperse oxide particles in the oxide films and increase the effective particle number density (N_0). It has been demonstrated that intensive melt shearing disperses the native MgO particles and increases the N_0 of MgO from 10^{14} m^{-3} (non-sheared) to 10^{17} m^{-3} (sheared) [32], with a three-order magnitude increase in particle number density. Here, we assume that the N_0 of Al_2O_3 particles increases from 10^{12} m^{-3} to 10^{15} m^{-3} after intensive melt shearing.

Without intensive melt shearing ($N_0(Al_2O_3) = 10^{12}$ m^{-3}), the predicted grain size of Al-4Cu alloy solidified at $\dot{T}$ = 3.5 K/s is 223 μm, while with intensive melt shearing ($N_0(Al_2O_3) = 10^{15}$ m^{-3}), the grain size is reduced to 85 μm. When 0.1 wt.% Al-5Ti-1B is added to the non-sheared Al-4Cu melt, there are two types of particles: potent TiB_2 ($N_0 = 7.3 \times 10^{12}$ m^{-3}) and Al_2O_3 ($N_0 = 10^{12}$ m^{-3}). Figure 3a is the calculated cooling curve for this case at $\dot{T}$ = 3.5 K/s, where both potent TiB_2 and Al_2O_3 particles nucleate α-Al and take part in the grain initiation process. Grain initiation by potent TiB_2 is typical PGI, whereas grain initiation by Al_2O_3 is HGI (Figure 3b). The calculated total grain number density (N) is 1.29×10^{12} m^{-3} (corresponding to a grain size of 73 μm), and most of the grains (99.99%) are initiated by potent TiB_2 particles. This means that the grain initiation is dominated by TiB_2 particles. When the addition of 0.1 wt.% Al-5Ti-1B grain refiner to the intensive melt sheared Al-4Cu melt, the calculated total number of grain initiation events (N) is 1.39×10^{12} m^{-3} (corresponding to a grain size of 71 μm), of which 89.7% grains are initiated by potent TiB_2 particles.

In this case (Figure 3), since ΔT_{max} (0.37 K) is greater than the nucleation undercooling (ΔT_n) for both potent TiB_2 (ΔT_n = 0.01 K) and the native Al_2O_3 particles (ΔT_n = 0.3 K), both potent TiB_2 and the native Al_2O_3 particles can participate in the nucleation process, although nucleation occurs on potent TiB_2 particles first and then on native Al_2O_3 particles. Besides the competition for nucleation, there is also a competition for grain initiation between the solid particles nucleated on both TiB_2 and Al_2O_3 particles, depending only on the particle size according to the free growth criterion (Equation (1)). Due to the much larger size of potent TiB_2 particles (d_0 = 0.68 μm for TiB_2 and d_0 = 0.08 μm for Al_2O_3) and the similar particle number density, the grain initiation process is dominated by TiB_2-nucleated solid particles, and only a small number of grain initiation events originate from Al_2O_3 particles (Figure 3c).

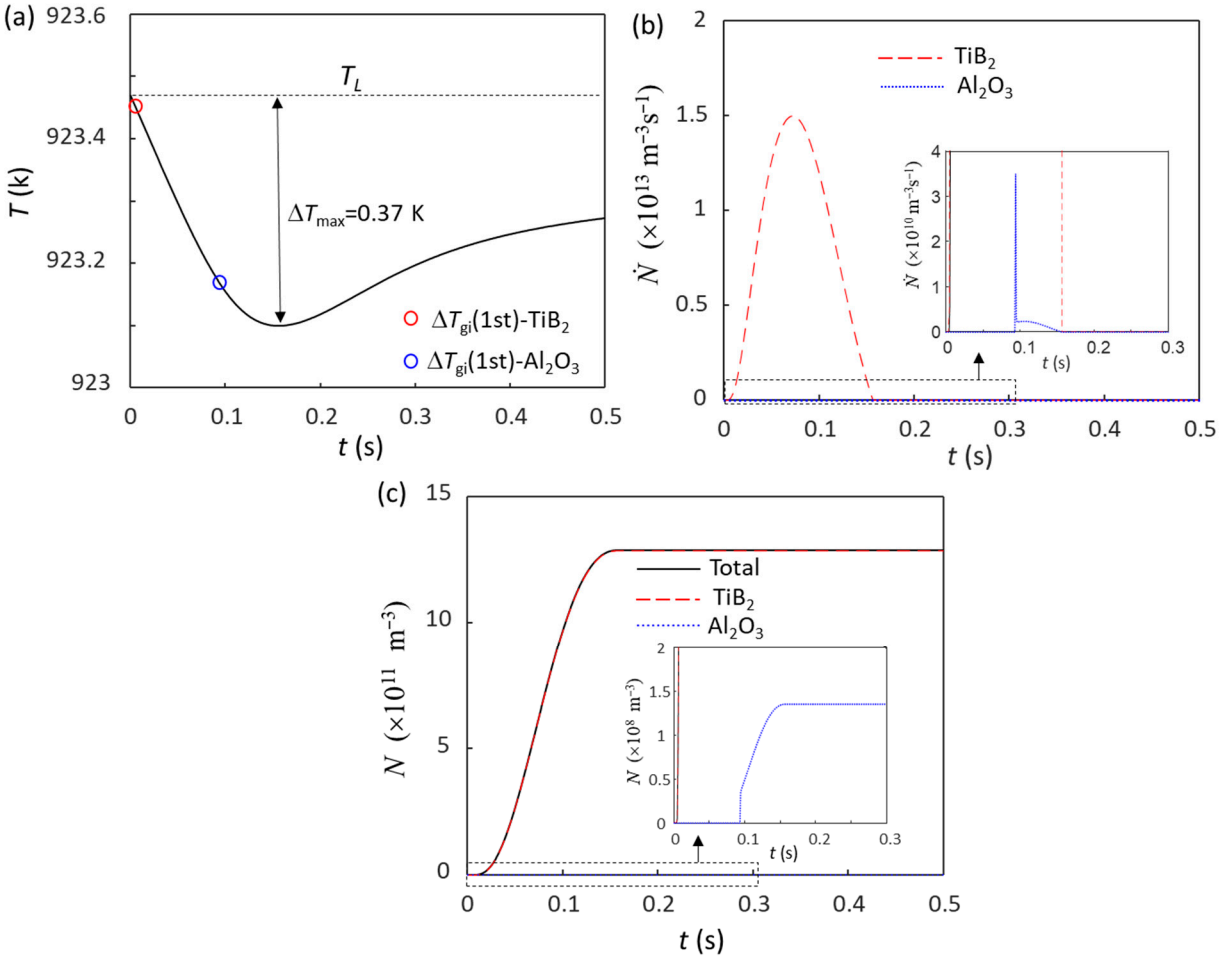

Figure 3. Solidification behavior of Al-4Cu alloy at $\dot{T}$ = 3.5 K/s with the addition of 0.1 wt.% Al-5Ti-1B grain refiner. (**a**) Cooling curve; (**b**) grain initiation rate; (**c**) initiated grain number density. The red and blue dots in (**a**) mark the onset of grain initiation on solid particles induced by TiB_2 and Al_2O_3 particles, respectively.

These results suggest that, with the addition of 0.1 wt.% Al-5Ti-1B grain refiner, potent TiB_2 particles dominate the grain initiation process and dictate the final grain size, making the number density of Al_2O_3 particles insignificant for grain refinement.

4.2. Competition for Grain Initiation between Zr and MgO Particles in Mg Alloys

The commercial Mg-33Zr grain refiner contains a large number of potent Zr particles which have a log-normal distribution with d_0 = 0.73 μm and σ = 0.62 [62]. The total number of Zr particles in the Mg-33Zr master alloy (N_0(Zr)) is estimated to be 10^{17} m^{-3}. There would be no Zr solid particles in Mg-Zr alloy melt if the Zr addition was less than 0.45 wt.%, the peritectic point (C_m) in the Mg-Zr binary system [59]. Therefore, for Mg-Zr alloys containing less than 0.45 wt.% Zr, the native MgO particles are the only nucleation sites. The number density of the native MgO particles (N_0(MgO)) in the Mg alloys has been estimated to be 10^{14} m^{-3} in the non-sheared melt and 10^{17} m^{-3} in the sheared melt [32].

Here, we analyze the solidification behavior of Mg-0.3Zr alloy, where 0.3 wt.% Zr provides sufficient growth restriction to deliver columnar to equiaxed transition (CET). Figure 4 shows the calculated cooling curves and grain initiation rates for Mg-0.3Zr alloy without and with intensive melt shearing. Without intensive melt shearing (N_0(MgO) = 10^{14} m^{-3}), the first batch of grain initiation events occur at the time of nucleation (blue circle in Figure 4a) and have a grain density of (7.1 × 10^8 m^{-3}), as shown in Figure 4b. Since these grain initiation events are not sufficient to cause recalescence, the melt temperature contin-

ues to decrease, and more grain initiation events can occur before recalescence (Figure 4b). The total grain density is 7.55 × 10^9 m^{-3} (corresponding to a grain size of 404 μm), of which only 9.4% of grains are initiated by EGI (the first batch), meaning that this is a PGI-dominant process [54,57]. With intensive melt shearing (N_0 = 10^{17} m^{-3}), the first (batch) grain initiation events (7.33 × 10^{11} m^{-3}) also occur at the time of nucleation, but unlike the case without intensive melt shearing, these grain initiation events are sufficient to cause recalescence, leading to a sharp increase in temperature (Figure 4a). This is a typical EGI process, as shown in Figure 4b. The grain size, in this case, is 88 μm, which is much finer than that without intensive melt shearing (404 μm).

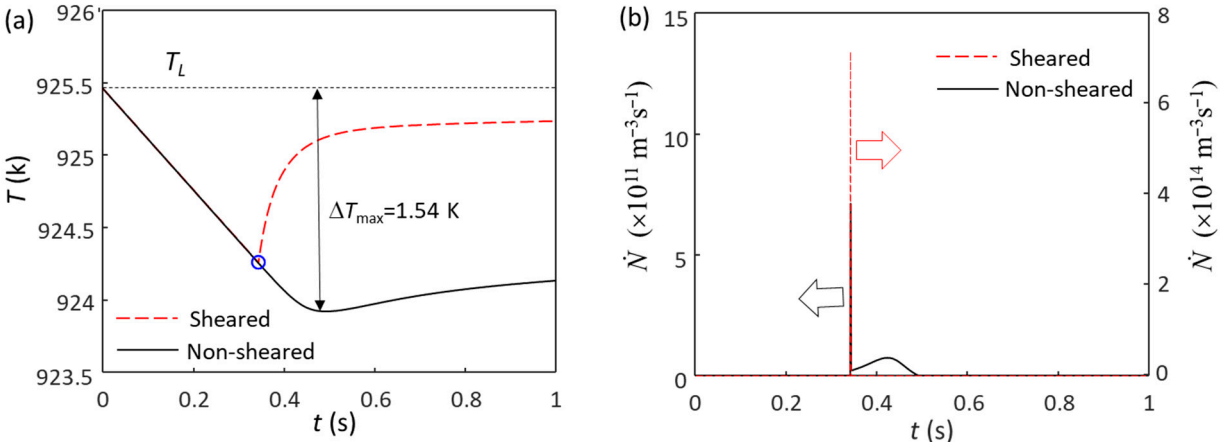

Figure 4. The calculated (**a**) cooling curves and (**b**) grain initiation rates of Mg-0.3Zr alloy without and with intensive melt shearing at a cooling rate of 3.5 K/s. The blue circle marks the onset of grain initiation induced by native MgO particles, which is also the nucleation temperature of native MgO nucleating α-Mg. The blue circle in (**a**) marks the onset of grain initiation on solid particles induced by MgO particles.

When the addition of Zr in the Mg-Zr alloys is slightly more than C_m, there exist undissolved (or primarily solidified) Zr particles, with the size distribution being assumed to be the same as that in the Mg-33Zr master alloy in this work. Therefore, there are two types of particles available for nucleation and grain initiation in the melt: the solid Zr particles and the native MgO particles.

For example, when the Zr content is 3.3 ppm larger than 0.45 wt.%, the estimated Zr particle number density in the Mg-Zr alloy melt is N_0 = 1 × 10^{11} m^{-3} (Mg-0.45Zr alloy with extra solid Zr particles). The calculated cooling curve for this alloy without intensive melt shearing is shown in Figure 5a. In this case, the grain initiation events start with Zr-induced solid particles, followed by MgO-induced solid particles, due to the larger particle size of Zr (d_0 = 0.73 μm for Zr and d_0 = 0.07 μm for MgO). Because of its low number density (1 × 10^{11} m^{-3}), the nucleation and grain initiations by Zr particles do not lead to recalescence. This provides an opportunity for MgO particles to participate in both the nucleation and grain initiation processes (Figure 5b) until recalescence at ΔT_{max} = 1.32 K. The grain initiation induced by Zr particles is a typical PGI, and that induced by MgO is an HGI (Figure 5b). If the Zr content is 5 ppm more than C_m (the N_0 of Zr particles is 1.5 × 10^{11} m^{-3}), the ΔT_{max} is 1.2 K (Figure 5c), which can just trigger the nucleation and grain initiation by MgO particles. The grain initiation induced by Zr particles is still PGI, but that induced by MgO becomes EGI, as shown in Figure 5d. The resultant grain size is 165 μm, and almost all the grains (99.3%) originate from Zr particles. With a slight further increase in the Zr content (assuming the N_0 of Zr particles is 1.6 × 10^{11} m^{-3}), the ΔT_{max} decreases to 1.19 K (Figure 5e), which cannot trigger the nucleation on MgO particles; then, the grains are all induced by Zr particles (Figure 5f). The increased addition of Zr will continue to increase the N_0 of Zr particles, and ΔT_{max} becomes smaller, so the MgO particle will have no chance to nucleate. From these three cases, for non-sheared Mg-0.45Zr

alloy, the addition of Zr particles ($N_0 > 1 \times 10^{11}$ m^{-3}) changes the grain initiation from MgO-dominant to Zr-dominant (see Table 2), accompanying a decrease in grain size with an increase in Zr particle number density.

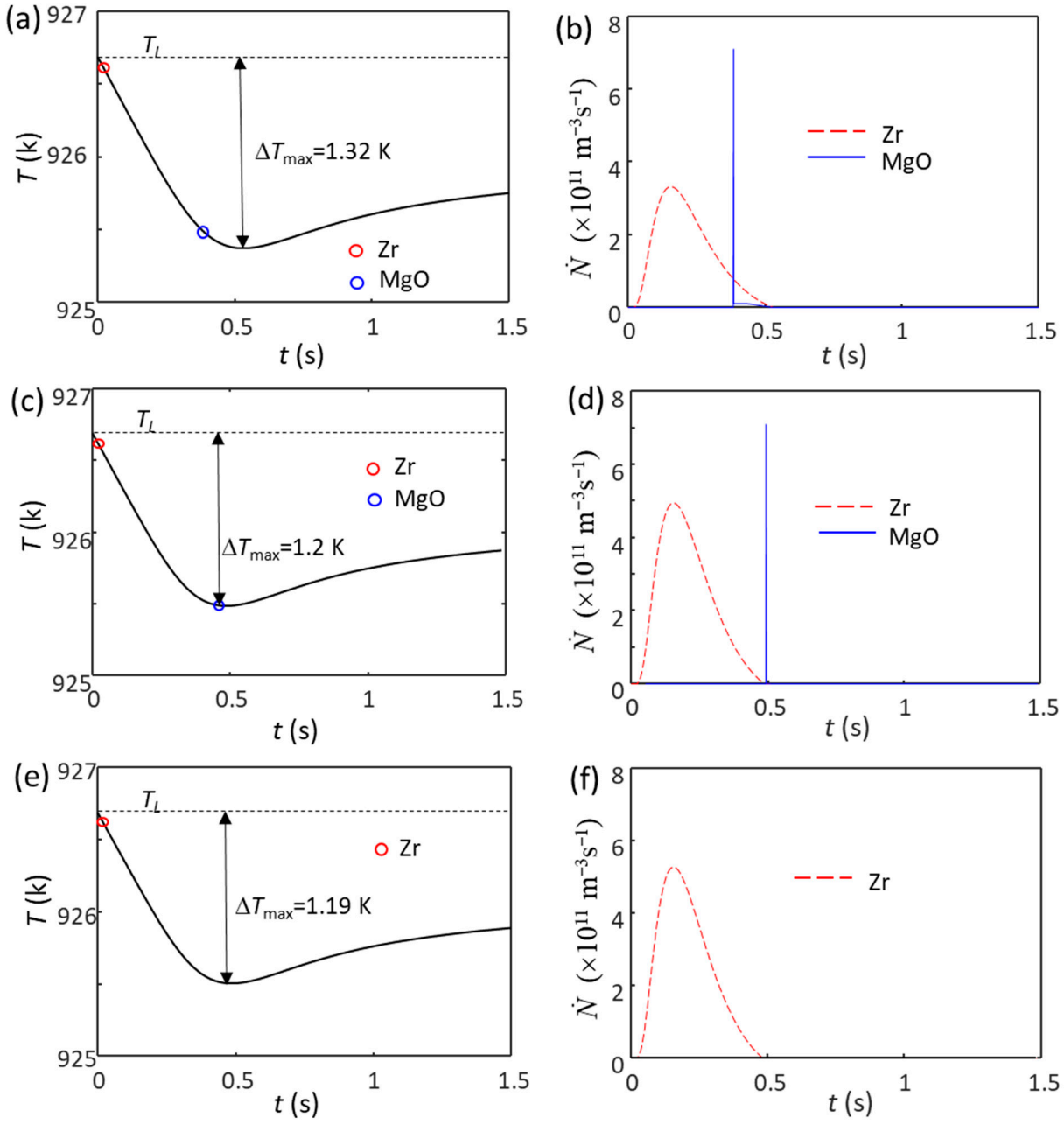

Figure 5. The calculated cooling curves (**a**,**c**,**e**) and grain initiation rates (**b**,**d**,**f**) of Mg-0.45Zr alloy with different amounts of Zr particles and without intensive melt shearing at a cooling rate of 3.5 K/s. (**a**,**b**) $N_0 = 1 \times 10^{11}$ m^{-3}, (**c**,**d**) $N_0 = 1.5 \times 10^{11}$ m^{-3}, (**e**,**f**) $N_0 = 1.6 \times 10^{11}$ m^{-3}. All the Zr particles are assumed to have the same log-normal size distribution (d_0 = 0.73 μm and σ = 0.62 (data from Ref. [62])). The red and blue circles mark the onset of grain initiation on solid particles induced by Zr and MgO particles, respectively.

Table 2. The calculated results of Mg-Zr alloys (the Zr content is slightly higher than C_m 0.45 wt.%) without and with intensive melt shearing prior to the addition of Zr particles. N_0(MgO) = 1.0×10^{14} for non-sheared melt and N_0(MgO) = 1.0×10^{17} m^{-3} for sheared melt.

N_0(Zr) (m^{-3})	N_0(MgO) (m^{-3})	ΔT_{max} (K)	N(Zr)/N	Grain Size (μm)
-	1.0×10^{14}	1.82	0	251
1.0×10^{11}	1.0×10^{14}	1.32	97.7%	184
1.5×10^{11}	1.0×10^{14}	1.2	99.3%	165
1.6×10^{11}	1.0×10^{14}	1.19	100%	162
-	1.0×10^{17}	1.2	0	88
1.0×10^{11}	1.0×10^{17}	1.2	9.2%	86
1.5×10^{11}	1.0×10^{17}	1.2	13.4%	85
1.6×10^{11}	1.0×10^{17}	1.19	100%	162

Note: N(Zr)/N represents the ratio of grain initiation events induced by Zr particles.

There is a critical particle number density of Zr (N_0*). When $N_0 \leq N_0$*, the recalescence will not occur before nucleation on MgO particles, and MgO particles will nucleate and take part in the grain initiation during solidification. When $N_0 > N_0$*, the recalescence will occur before nucleation by MgO due to the sufficient number of Zr particles taking part in the grain initiation. Hence, the MgO particles have no chance to nucleate, failing in the competition for nucleation.

Figure 6 shows the solidification behavior of sheared Mg-Zr alloy with 3.3 ppm extra Zr (N_0(Zr) = 1×10^{11} m^{-3}). The first batch of grain initiation events are induced by Zr particles (Figure 6a), being the same as the case of the non-sheared alloy (Figure 5a). Because of the high N_0 of MgO particles resulting from intensive melt shearing, once nucleation occurs on MgO particles, a large number of them can initiate grains, resulting in an immediate recalescence (Figure 6b), which is a typical EGI by MgO particles, and the ΔT_{max} is 1.2 K. However, unlike the case without intensive melt shearing, about 90.8% of the grains are induced in EGI by MgO particles. As a result, the corresponding grain size is 86 μm, which is slightly smaller than that of Mg-0.45Zr alloy with intensive melt shearing but without Zr particles (Table 2). The grain size only slightly decreases with the increase in the Zr particles until N_0 = 1.5×10^{11} m^{-3}. Figure 7 shows the grain size as a function of Zr content in Mg-Zr alloys without and with intensive melt shearing. When the N_0 of Zr particles is increased to 1.6×10^{11} m^{-3}, ΔT_{max} is 1.19 K, and the grain initiation is only induced by Zr particles, as shown in Figure 5e. In this case, the grain size is 162 μm, which is much larger than that (85 μm) when the N_0 of Zr particles is 1.5×10^{11} m^{-3} (Figure 7). Only when the N_0 of Zr particles continues to increase can the grain size decrease (Figure 7). When the Zr content is less than 0.45 wt.% (C_m), it is assumed that there are no Zr particles in the melt; when the Zr content is larger than 0.45 wt.%, there will be Zr particles in the melt, and the N_0 of Zr particles is calculated from the excess Zr based on the assumption that the Zr particles in the melt have the same size distribution as that in the Mg-33Zr grain refiner. It should be noted that, in the real cases, the N_0 of the Zr particles is most likely lower than the calculated value, especially for the melt with intensive melt shearing, because the intensive melt shearing will promote the coarsening of the Zr particles in the melt [34].

For the Mg-Zr alloys with a Zr content less than C_m, the native MgO particles are the only solid particles, and they will participate in the nucleation and grain initiation. The grain size decreases with increasing Zr content due to the increase in growth restriction, as shown in Figure 7. Note that the grain size without intensive melt shearing decreases more readily than that with intensive melt shearing because the solidification of alloys without intensive melt shearing is PGI-dominant, whereas that with intensive melt shearing is EGI-dominant (Figure 4). It is also noticed that the growth restriction effect of Zr on the grain size is stronger for PGI-dominant than EGI-dominant [54,57].

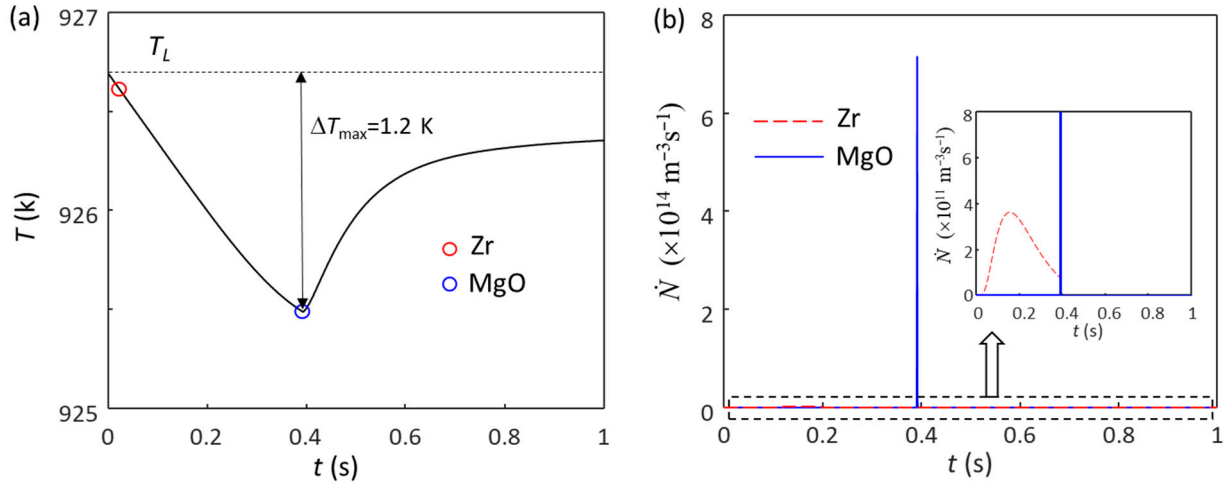

Figure 6. The calculated (**a**) cooling curve and (**b**) grain initiation rate of sheared Mg-0.45Zr alloy with a small number of Zr particles ($N_0 = 1 \times 10^{11}$ m^{-3}) at a cooling rate of 3.5 K/s. The red and blue circles mark the onset of grain initiation on solid particles induced by Zr and MgO particles, respectively.

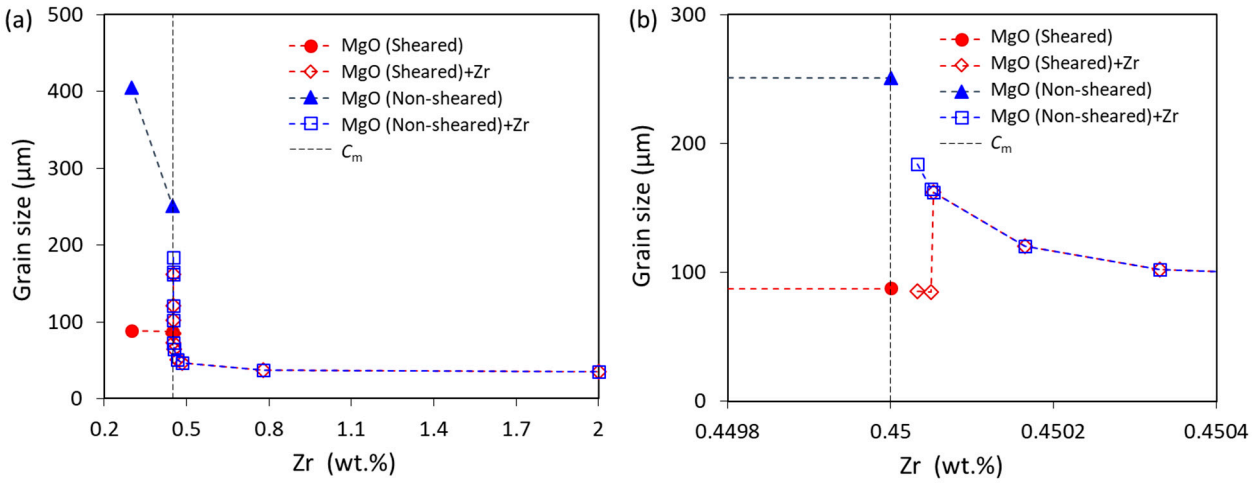

Figure 7. (**a**) The calculated grain size of Mg-Zr alloys with and without intensive melt shearing at a cooling rate of 3.5 K/s; and (**b**) the enlarged part of (**a**) with a Zr concentration near C_m. The N_0 of Zr particles is equivalent to the extra Zr (exceeding 0.45 wt.%) based on the size distribution of Zr in the Mg-33Zr grain refiner.

When the Zr content in Mg-Zr alloys is more than C_m, Zr particles will be available for the nucleation of α-Mg, and then the Zr particles and native MgO particles co-exist in the melt. There will be competition for nucleation and grain initiation during solidification. As shown in Figure 5 for the non-sheared melt (N_0 of MgO is 10^{14} m^{-3}), when the N_0 of Zr particles is less than 1.5×10^{11} m^{-3}, both Zr and MgO particles will participate in nucleation and grain initiation. However, when the N_0 of Zr particles is more than 1.5×10^{11} m^{-3}, only Zr particles participate in nucleation and grain initiation, and MgO particles fail in the competition. The grain size of the non-sheared melt continuously decreases with the increase in Zr addition because of the increase in growth restriction (Zr content < C_m) and Zr particle number density (Zr content > C_m) (Figure 7).

For the sheared melt (N_0 of MgO is 10^{17} m^{-3}), both Zr and MgO particles participate in nucleation and grain initiation when the N_0 of Zr particles is less than 1.5×10^{11} m^{-3}, which is the same with the non-sheared melt but with a smaller grain size (Figure 7a). When the N_0 of Zr particles is 1.6×10^{11} m^{-3}, MgO particles fail in the competition for nucleation. In this case, only Zr particles participate in nucleation and grain initiation,

increasing the grain size (Figure 7b). With the further addition of Zr, the grain size then decreases due to the increase in Zr particles in the melt (Figure 7a).

It should be pointed out that the grain size is the same for both the non-sheared and sheared melt when the N_0 of Zr particles is more than 1.5×10^{11} m^{-3} (corresponding to 5 ppm extra Zr), as MgO particles fail to win the competition for nucleation under this condition. However, in the case of experiments under such conditions [34], the resultant grain sizes are different for the samples with and without melt shearing, because intensive melt shearing promotes the coarsening of the Zr particles in the melt, resulting in the difference in the Zr particle number density in the non-sheared and sheared melts [34]. Overall, the grain size data are qualitatively in good agreement between the calculations (Figure 7) and experiments [34].

5. General Discussion

From the previous analysis, even though two (or more than two) types of particles co-exist in the melt, it is possible that only one type of particle can participate in the nucleation and grain initiation due to the large difference in ΔT_n. This means that there exists competition for nucleation and grain initiation among the different types of particles during solidification. Assuming that there are two types of particles in the melt—Type 1 particles with a nucleation undercooling of $\Delta T_n(1)$, and Type 2 particles with a nucleation undercooling of $\Delta T_n(2)$—we have the following four cases for competition for nucleation between these two types of particles depending on the relative positions of their nucleation undercoolings to the maximum achievable undercooling during solidification, ΔT_{max}:

- when $\Delta T_n(1) < \Delta T_{max} < \Delta T_n(2)$, only Type 1 particles participate in nucleation;
- when $\Delta T_n(2) < \Delta T_{max} < \Delta T_n(1)$, only Type 2 particles participate in nucleation;
- when $\Delta T_n(1) < \Delta T_n(2) < \Delta T_{max}$, both Type 1 and Type 2 particles participate in nucleation; Type 1 particles nucleate first, followed by Type 2 particles; and
- when $\Delta T_n(2) < \Delta T_n(1) < \Delta T_{max}$, both Type 1 and Type 2 particles participate in nucleation; Type 2 particles nucleate first, followed by Type 1 particles.

Such competition for nucleation is schematically illustrated in Figure 8, where the $\Delta T_n(1) - \Delta T_n(2)$ plot is divided into four different zones by three characteristic lines: the black dotted line for $\Delta T_n(1) = \Delta T_n(2)$; the red dashed line for $\Delta T_n(2) = \Delta T_{max}$; and the blue dashed line for $\Delta T_n(1) = \Delta T_{max}$. The four zones represent different characteristics of nucleation. Effectively, Figure 8 becomes a nucleation competition map, which can be used to facilitate the understanding of nucleation competition.

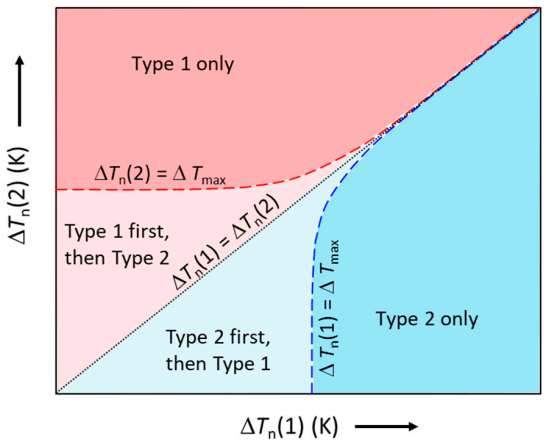

Figure 8. Schematic illustration of the competition for nucleation between two types of particles (Type 1 and Type 2). The red and blue dashed lines represent $\Delta T_n(2) = \Delta T_{max}$ and $\Delta T_n(1) = \Delta T_{max}$, respectively; the black dotted line represents $\Delta T_n(1) = \Delta T_n(2)$. In the red area, only Type 1 particles nucleate; in the blue area, only Type 2 particles nucleate; in the light red area, Type 1 particles nucleate first, followed by Type 2 particles; in the light blue area, Type 2 particles nucleate first, followed by Type 1 particles.

Therefore, in a system with different types of particles, the basic rule governing the competition for nucleation can be expressed as:

$$\Delta T_n = Min\{\Delta T_n(i)\} \text{ and } \Delta T_n(i) < \Delta T_{max} \quad (3)$$

where $\Delta T_n(i)$ is the nucleation undercooling required by the ith type of nucleant particles. As heterogeneous nucleation is a deterministic process and independent of particle size, nucleation occurs first on nucleant particles with the smallest nucleation undercooling and then on particles with progressively larger nucleation undercoolings. This process continues until recalescence (ΔT_{max}), which denies the chance for heterogeneous nucleation on those particles that have not participated in nucleation so far.

It should be noted that nucleation does not mean grain initiation. Although both Type 1 and Type 2 particles in the light red and light blue zones in Figure 8 can nucleate, whether both of them can participate in the subsequent grain initiation process is dependent on their sizes. In other words, the competition for grain initiation only occurs on those particles that have participated in heterogeneous nucleation. After nucleation, all the nucleant particles become solid particles. According to the free growth criterion [53], grain initiation is only related to the sizes of solid particles and is independent of the nature of the substrate, such as misfit, surface roughness and chemistry. Therefore, the competition for grain initiation is among all those solid particles and is irrelevant to the substrates on which the solid particles were nucleated. Hence, we have the following competition rule for grain initiation:

$$\Delta T_{gi} = Max\{d_N(i)\} \quad (4)$$

where $d_N(i)$ is the diameter of the ith nucleant particles that have already participated in nucleation. Equation (4) states that, among all the solid particles, the largest solid particles initiate the grain first, followed by grain initiation on progressively smaller ones regardless of the type of the nucleant particles, as long as nucleation has occurred in the first place.

This competition rule for grain initiation is schematically illustrated in Figure 9, which shows a hypothetical melt containing three different types of nucleant particles (denoted as A, B and C) with their unique size distributions. It is also assumed that all three types of nucleant particles have already participated in heterogeneous nucleation (i.e., $\Delta T_n(i) \leq \Delta T_{max}$). After nucleation, a spherical cap is created on a nucleant particle, forming a solid particle which has the same size as the nucleant particle. Therefore, the size distribution of solid particles from each type of nucleant particle is the same as that of the nucleant particles. The corresponding grain initiation undercooling is also shown in Figure 9, from which we obtain the minimum substrate size, d_{min}, which corresponds to the maximum achievable undercooling (e.g., limited by recalescence), ΔT_{max}. Clearly, only those nucleant particles with their size $d_N \geq d_{min}$ are able to initiate grains. This means that, as shown in Figure 9, all of the C type particles and some of the B type particles contribute to grain initiation, whilst all of the A type particles will not participate in grain initiation.

The traditional wisdom to achieve grain refinement is to enhance heterogeneous nucleation by the addition of potent nucleant particles (i.e., to reduce ΔT_n) to alloy melts prior to solidification, as demonstrated by chemical inoculation with Al-5Ti-1B grain refiner in Al alloys and with Mg-Zr grain refiner in Mg alloys. This approach is to improve the competitiveness of the exogenous particles from grain refiners for nucleation and grain initiation by enhancing their nucleation potency and/or increasing the particle number density. This approach promotes PGI and leaves little space for further improvement in grain refinement efficiency [54,56,57].

The concept of explosive grain initiation (EGI) provides a new approach to enhancing the efficiency of grain refinement: more significant grain refinement can be achieved by promoting EGI through impeding heterogeneous nucleation [54,56,57]. Many native oxide particles exist in Al and Mg alloy melts. Once made available by high shear, they deliver effective grain refinement, as demonstrated by the intensive melt shearing in Al-Mg alloys [13] and Mg-Al alloys [12]. As shown in Section 4, the well-dispersed Al_2O_3 particles

can lead to a decrease in the grain size of Al-4Cu alloy from 223 to 85 μm, comparable with the addition of 0.1 wt.% Al-5Ti-1B grain refiner (the grain size is 73 μm). For Mg alloys, the addition of a small amount of Mg-Zr grain refiner to the melts with intensive melt shearing may lead to an increase in the grain size (Figure 7b). The addition of sufficient grain refiner can deliver a grain size comparable to that achieved by the native MgO particles (Figure 7). However, grain refinement obtained by inoculation not only increases the cost but also makes recycling more difficult. Furthermore, their existence at grain boundaries deteriorates the mechanical performance of the as-cast components.

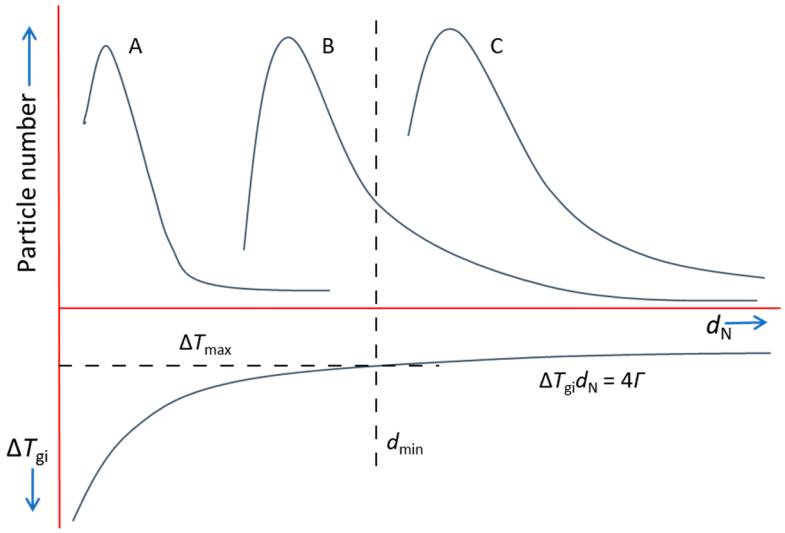

Figure 9. Schematic illustration of the competition for grain initiation between three different types of nucleant particles (denoted as A, B and C), with their unique size distributions. We assumed that all three types of particles have participated in nucleation. d_{min} is the minimum solid particle size determined from the maximum undercooling (ΔT_{max}).

The challenge for grain-refining Al and Mg alloys using the native oxide particles is to make the native oxide particles dominate the nucleation and grain initiation processes. This can be achieved by: (1) eliminating other, more potent impurity particles of a significant number density in the melt; and (2) increasing the number density of oxide particles to change the grain initiation by native oxide particles from PGI-dominant to EGI-dominant. In this sense, the intensive melt shearing technique that can effectively disperse native oxide particles in the melt is particularly useful for the grain refinement of Al and Mg alloys [12–16,63–65]. However, it should be pointed out that any technique that can effectively disperse the oxide films in the melts can deliver grain refinement. Besides dispersing native oxide particles, another approach to further grain refinement is to reduce the nucleation potency of the native oxide particles by altering the lattice misfit and/or introducing interfacial roughness [54,56,57].

6. Summary

In this paper, we studied the competition for nucleation and grain initiation in melts containing more than one type of particle. Using a numerical model, we have analyzed the competition in Al-Cu alloys inoculated with Al-5Ti-1B grain refiner and Mg-Zr alloys inoculated with Mg-Zr grain refiner. Based on the numerical results, we have developed the basic rules of competition for nucleation and grain initiation in the systems containing more than one type of nucleant particle:

(1) The competition for heterogeneous nucleation is governed by $\Delta T_n = Min\{\Delta T_n(i)\}$, which states that nucleation occurs first on nucleant particles with the smallest nucleation undercooling and then on particles with progressively smaller nucleation undercoolings until recalescence.

(2) The competition for grain initiation occurs only on those particles that have participated in heterogeneous nucleation and is governed by $\Delta T_{gi} = Max\{d_N(i)\}$, which states that, among all the solid particles, the largest solid particles initiate grains first, followed by grain initiation on progressively smaller ones regardless of the type of nucleant particles from which the solid particles originated.

In addition, we have demonstrated that well-dispersed native oxide particles by intensive melt shearing can reduce the grain size to a level that is comparable with that achieved by the addition of a grain refiner.

Author Contributions: Conceptualization, Z.F. and F.G.; methodology, F.G.; validation, F.G.; formal analysis, F.G.; investigation, F.G.; resources, F.G.; data curation, F.G.; writing—original draft preparation, F.G.; writing—review and editing, Z.F.; visualization, F.G.; supervision, Z.F.; project administration, Z.F.; funding acquisition, Z.F. All authors have read and agreed to the published version of the manuscript.

Funding: This work was financially supported by the EPSRC (UK) under grant number EP/N007638/1.

Data Availability Statement: Not applicable.

Conflicts of Interest: The authors declare no conflict of interest.

References

1. Kelton, K.F.; Greer, A.L. (Eds.) *Nucleation in Condensed Matter: Applications in Materials and Biology*; Pergamon: Oxford, UK, 2010.
2. McCartney, D.G. Grain refining of Al and its alloys using inoculants. *Int. Mater. Rev.* **1989**, *34*, 247–260. [CrossRef]
3. Easton, M.; StJohn, D. Grain refinement of aluminum alloys: Part I. The nucleant and solute paradigms—A review of the literature. *Metall. Mater. Trans. A* **1999**, *30*, 1613–1623. [CrossRef]
4. Murty, B.S.; Kori, S.A.; Chakraborty, M. Grain refinement of aluminium and its alloys by heterogeneous nucleation and alloying. *Int. Mater. Rev.* **2002**, *47*, 3–29. [CrossRef]
5. Easton, M.A.; Qian, M.; Prasad, A.; StJohn, D.H. Recent advances in grain refinement of light metals and alloys. *Curr. Opin. Solid State Mater. Sci.* **2016**, *20*, 13–24. [CrossRef]
6. Ralston, K.D.; Birbilis, N. Effect of grain size on corrosion: A review. *Corrosion* **2010**, *66*, 075005–075005-13. [CrossRef]
7. Czerwinski, F. (Ed.) *Magnesium Alloys—Design, Processing and Properties*; InTech: Rijeka, Croatia, 2011.
8. Eskin, D.G.; Tzanakis, I.; Wang, F.; Lebon, G.S.B.; Subroto, T.; Pericleous, K.; Mi, J. Fundamental studies of ultrasonic melt processing. *Ultrason. Sonochemistry* **2019**, *52*, 455–467. [CrossRef] [PubMed]
9. Jaroszewski, M.; Thomas, S.; Rane, A.V. (Eds.) *Advanced Materials for Electromagnetic Shielding: Fundamentals, Properties, and Applications*; John Wiley & Sons: Hoboken, NJ, USA, 2019.
10. Zhang, L.; Wang, S.; Dong, A.; Gao, J.; Damoah, L.N.W. Application of electromagnetic (EM) separation technology to metal refining processes: A review. *Metall. Mater. Trans. B* **2014**, *45*, 2153–2185. [CrossRef]
11. Liu, L.; Chen, X.; Pan, F. A review on electromagnetic shielding magnesium alloys. *J. Magnes. Alloy.* **2021**, *9*, 1906–1921. [CrossRef]
12. Fan, Z.; Wang, Y.; Xia, M.; Arumuganathar, S. Enhanced heterogeneous nucleation in AZ91D alloy by intensive melt shearing. *Acta Mater.* **2009**, *57*, 4891–4901. [CrossRef]
13. Li, H.T.; Wang, Y.; Fan, Z. Mechanisms of enhanced heterogeneous nucleation during solidification in binary Al-Mg alloys. *Acta Mater.* **2012**, *60*, 1528–1537. [CrossRef]
14. Fan, Z.; Xia, M.; Zhang, H.; Liu, G.; Patel, J.B.; Bian, Z.; Bayandorian, I.; Wang, Y.; Li, H.T.; Scamans, G.M. Melt conditioning by advanced shear technology (MCAST) for refining solidification microstructures. *Int. J. Cast Met. Res.* **2009**, *22*, 103–107. [CrossRef]
15. Fan, Z.; Zuo, Y.B.; Jiang, B. A new technology for treating liquid metals with intensive melt shearing. *Mater. Sci. Forum* **2011**, *690*, 141–144. [CrossRef]
16. Patel, J.B.; Yang, X.; Mendis, C.L.; Fan, Z. Melt conditioning of light metals by application of high shear for improved microstructure and defect control. *JOM* **2017**, *69*, 1071–1076. [CrossRef]
17. Fan, Z.; Zuo, Y.B.; Jiang, B. Apparatus and Method for Liquid Metals Treatment. International Patent Application No. PCT/GB2011/051744, 2010.
18. Ali, Y.; Qiu, D.; Jiang, B.; Pan, F.; Zhang, M.X. Current research progress in grain refinement of cast magnesium alloys: A review. *J. Alloys Compd.* **2015**, *619*, 639–651. [CrossRef]
19. Fan, Z.; Wang, Y.; Zhang, Y.; Qin, T.; Zhou, X.R.; Thompson, G.E.; Pennycook, T.; Hashimotob, T. Grain refining mechanism in the Al/Al-Ti-B system. *Acta Mater.* **2015**, *84*, 292–304. [CrossRef]
20. Engh, T.A. (Ed.) *Principles of Metal Refining*; Oxford University Press: Oxford, UK, 1992.
21. Sin, S.L.; Elsayed, A.; Ravindran, C. Inclusions in magnesium and its alloys: A review. *Inter. Mater. Rev.* **2013**, *58*, 419–436. [CrossRef]

22. Wang, F.; Fan, Z. Characterization of AlN inclusion particles formed in commercial purity aluminum. *Metall. Mater. Trans. A* **2019**, *50*, 2519–2526. [CrossRef]
23. Que, Z.; Mendis, C.L. Effects of native AlN particles on heterogeneous nucleation in an Al-3Fe alloy. *Metall. Mater. Trans. A* **2021**, *52*, 553–559. [CrossRef]
24. Bakke, P.; Karlsen, D.O. Inclusion assessment in magnesium and magnesium base alloys. *SAE Trans.* **1997**, *106*, 314–326.
25. Campbell, J. (Ed.) *Castings*, 2nd ed.; Butterworth-Heinemann: Oxford, UK, 2003.
26. Wu, G.; Dash, K.; Galano, M.L.; O'Reilly, K.A.Q. Oxidation studies of Al alloys: Part II Al-Mg alloy. *Corr. Sci.* **2019**, *155*, 97–108. [CrossRef]
27. Mirak, A.R.; Divandari, M.; Boutorabi, S.M.A.; Campbell, J. Oxide film characteristics of AZ91 magnesium alloy in casting conditions. *Int. J. Cast Met. Res.* **2007**, *20*, 215–220. [CrossRef]
28. Pettersen, G.; Øvrelid, E.; Tranell, G.; Fenstad, J.; Gjestland, H. Characterisation of the surface films formed on molten magnesium in different protective atmospheres. *Mater. Sci. Eng. A* **2002**, *332*, 285–294. [CrossRef]
29. Balart, M.J.; Fan, Z. Surface oxidation of molten AZ91D magnesium alloy in air. *Int. J. Cast Met. Res.* **2014**, *27*, 167–175. [CrossRef]
30. Wang, S.; Wang, Y.; Ramasse, Q.; Fan, Z. The nature of native MgO in Mg and its alloys. *Metall. Mater. Trans. A* **2020**, *51*, 2957–2974. [CrossRef]
31. Wang, Y.; Fan, Z.; Zhou, X.; Thompson, G.E. Characterisation of magnesium oxide and its interface with α-Mg in Mg-Al-based alloys. *Phil. Mag. Lett.* **2011**, *91*, 516–529. [CrossRef]
32. Men, H.; Jiang, B.; Fan, Z. Mechanisms of grain refinement by intensive shearing of AZ91alloy melt. *Acta Mater.* **2010**, *58*, 6526–6534. [CrossRef]
33. Fang, C.M.; Fan, Z. Prenucleation at the interface between MgO and liquid magnesium: An ab initio molecular dynamics study. *Metall. Mater. Trans. A* **2020**, *51*, 788–797. [CrossRef]
34. Peng, G.S.; Wang, Y.; Fan, Z. Competitive heterogeneous nucleation between Zr and MgO particles in commercial purity magnesium. *Metall. Mater. Trans. A* **2018**, *49*, 2182–2192. [CrossRef]
35. Gibbs, J.W. On the equilibrium of heterogeneous substances. *Am. J Sci.* **1879**, *16*, 441–458. [CrossRef]
36. Volmer, M.; Weber, A.Z. Nucleus formation in supersaturated systems. *Z. Für Phys. Chem.* **1926**, *119*, 277–301. [CrossRef]
37. Becker, R.; Döring, W. Kinetic treatment of nucleation in supersaturated vapors. *Ann. Phys.* **1935**, *24*, 719–752. [CrossRef]
38. Zeldovich, J.B. On the theory of new phase formation: Cavitation. *Acta Physicochim. USSR* **1943**, *18*, 1–22.
39. Kashchiev, D. *Nucleation: Basic Theory with Applications*; Butterworth-Heinemann: Oxford, UK, 2000.
40. Cantor, B. Heterogeneous nucleation and adsorption. *Phil. Trans. R. Soc. Lond. A* **2003**, *361*, 409–417. [CrossRef]
41. Kim, W.T.; Cantor, B. Solidification behaviour of Pb droplets embedded in a Cu matrix. *Acta Metal. Mater.* **1992**, *40*, 3339–3347. [CrossRef]
42. Kim, W.T.; Cantor, B. Heterogeneous nucleation of Al2Cu in Al-Cu eutectic liquid droplets embedded in an al matrix. *Acta Metal. Mater.* **1994**, *42*, 3045–3053. [CrossRef]
43. Fan, Z. An Epitaxial model for heterogeneous nucleation on potent substrates. *Metall. Mater. Trans. A* **2013**, *44*, 1409–1418. [CrossRef]
44. Men, H.; Fan, Z. Prenucleation induced by crystalline substrates. *Metall. Mater. Trans. A* **2018**, *49*, 2766–2777. [CrossRef]
45. Men, H.; Fang, C.M.; Fan, Z. Prenucleation at the liquid/substrate interface: An overview. *Metals* **2022**, *in progress*.
46. Jiang, B.; Men, H.; Fan, Z. Atomic ordering in the liquid adjacent to an atomically rough solid surface. *Comp. Mater. Sci.* **2018**, *153*, 73–81. [CrossRef]
47. Fang, C.M.; Men, H.; Fan, Z. Effect of substrate chemistry on prenucleation. *Metall. Mater. Trans. A* **2018**, *49*, 6231–6242. [CrossRef]
48. Fan, Z.; Men, H. A molecular dynamics study of heterogeneous nucleation in generic liquid/substrate systems with positive lattice misfit. *Mater. Res. Express* **2020**, *7*, 126501. [CrossRef]
49. Fan, Z.; Men, H.; Wang, Y.; Que, Z.P. A new atomistic mechanism for heterogeneous nucleation in the systems with negative lattice misfit: Creating a 2D template for crystal growth. *Metals* **2021**, *11*, 478. [CrossRef]
50. Fan, Z.; Men, H. Heterogeneous nucleation and grain initiation on a single substrate. *Metals* **2022**, *12*, 1454. [CrossRef]
51. Fan, Z.; Men, H. An overview on atomistic mechanisms of heterogeneous nucleation. *Metals* **2022**, *in progress*.
52. Turnbull, D.; Vonnegut, B. Nucleation catalysis. *Ind. Eng. Chem.* **1952**, *44*, 1292–1298. [CrossRef]
53. Greer, A.L.; Bunn, A.M.; Tronche, A.; Evans, P.V.; Bristow, D.J. Modelling of inoculation of metallic melts: Application to grain refinement of Al by Al-Ti-B. *Acta Mater.* **2000**, *48*, 2823–2835. [CrossRef]
54. Fan, Z.; Gao, F.; Jiang, B.; Que, Z.P. Impeding nucleation for more significant grain refinement. *Sci. Rep.* **2020**, *10*, 9448. [CrossRef]
55. Quested, T.E.; Greer, A.L. The effect of the size distribution of inoculant particles on as-cast grain size in aluminium alloys. *Acta Mater.* **2004**, *52*, 3859–3868. [CrossRef]
56. Fan, Z. Heterogeneous nucleation, grain initiation and grain refinement of Mg-alloys. In Proceedings of the 11th International Conference on Magnesium Alloys and Their Applications, Old Winsor, UK, 24–27 July 2018; pp. 7–17.
57. Fan, Z.; Gao, F. Grain initiation and grain refinement: An overview. *Metals* **2022**, *in progress*.
58. Fan, Z.; Gao, F.; Zhou, L.; Lu, S.Z. A new concept for growth restriction during solidification. *Acta Mater.* **2018**, *152*, 248–257. [CrossRef]
59. Calculated from Pandat 2021 Version Software with PanMg Database. Available online: https://computherm.com/databases (accessed on 7 August 2022).

60. Wang, S.H.; Wang, Y.; Fan, Z. Brunel University London, Uxbridge, Middlesex, UK. *to be submitted*.
61. Wang, D.; Chang, W.; Shen, Y.; Sun, J.; Sheng, C.; Zhang, Y.; Zhai, Q. The role of lattice mismatch in heterogeneous nucleation of pure Al on Al_2O_3 single-crystal substrates with different termination planes. *J. Therm. Anal. Calorim.* **2019**, *137*, 791–797. [CrossRef]
62. Wang, Y.; Fan, Z. Grain refinement of Mg alloys by Zr. *to be submitted*.
63. Zuo, Y.B.; Jiang, B.; Zhang, Y.; Fan, Z. January. Grain refinement of DC cast magnesium alloys with intensive melt shearing. *IOP Conf. Ser. Mater. Sci. Eng.* **2012**, *27*, 012043.
64. Das, S.; Barekar, N.; El Fakir, O.; Yang, X.; Dear, J.P.; Fan, Z. Influence of intensive melt shearing on subsequent hot rolling and the mechanical properties of twin roll cast AZ31 strips. *Mater. Lett.* **2015**, *144*, 54–57. [CrossRef]
65. Fan, Z.; Wang, Y.; Zhang, Z.F.; Xia, M.; Li, H.T.; Xu, J.; Granasy, L.; Scamans, G.M. Shear enhanced heterogeneous nucleation in some Mg-and Al-alloys. *Int. J. Cast Met. Res.* **2009**, *22*, 318–322. [CrossRef]